MONITORING THE SURFACTANT-ENHANCED OIL DISSOLUTION AND MOBILIZATION IN POROUS MEDIA

C. Aggelopoulos[1], V. Sygouni[1], D. Tzovolou[1], M. Theodoropoulou[2], D.G. Avraam[3], C.D. Tsakiroglou[1]

[1]Foundation for Research and Technology Hellas-Institute of Chemical Engineering and High Temperature Chemical Processes, Stadiou str., Platani, 26504 Patras,Greece
[2]Department of Mechanical Engineering, TEI of Patras, 26334 Patras, Greece
[3]Department of Pollution Control Technologies, TEI of Western Macedonia, 50100 Kozani, Greece

This paper was prepared for presentation at the International Symposium of the Society of Core Analysts held in Noordwijk, The Netherlands 27-30 September, 2009

ABSTRACT

A fast and accurate method, based on multipoint electrical measurements, is used to monitor the hydrocarbon mobilization/dissolution in a porous medium, during the rate-controlled injection of a surfactant solution. The residual n-C_{10} remaining in a soil column after a fast drainage and a slow imbibition step is flushed by an aqueous solution of NaCl (17.5 g/L) and anionic surfactant SDS (4.9 g/L). The transient response of the water saturation averaged over five successive segments of the soil column is monitored by transforming the electrical resistance between five pairs of electrodes to water saturations with the aid of a non-Archie equation. The sequential mobilization and entrapment of n-C_{10} ganglia in the various segments are fast processes observed during the first stages of the flushing test, while the n-C_{10} dissolution in aqueous and SDS micelle phases is a slow process observed mainly during advanced stages of the test. A mathematical model of surfactant enhanced hydrocarbon dissolution and mobilization is developed. Based on the experimental data, an effective dissolution rate (EDR) is determined explicitly over each soil column segment. The EDR is the sum of the actual n-C_{10} dissolution rate and the net rate of n-C_{10} mass outflow through the soil segment.

INTRODUCTION

Surfactant-enhanced oil dissolution and mobilization belongs to the well-promising methods of (1) enhanced oil and condensate gas recovery, and (2) soil remediation (Khachikian and Harmon, 2000). Surfactants combine a characteristic structural group that has a strong attraction for oil together with a hydrophilic group which has a strong attraction to water (Zhou and Zhu, 2004). Surfactants are primarily used either to enhance dissolution of oil into aqueous phase or reduce the interfacial tension between oil/water. In the one case the mixture of oil and water is received as a single phase (Zhou et al., 2000) while in the second case the oil is mobilized as a separate phase (Chrysikopoulos and Vogler, 2006). At surfactant concentrations higher than the CMC (critical micelle concentration) the solubility of oils in the aqueous phase increase since oil molecules are captured and trapped (solubilized) into micelles (Prak et al., 1999). For ionic surfactants where the micelles and oil drops repel, it is generally accepted that oil molecules dissolve and diffuse away from the interface, subsequently being

incorporated into micelles either during their traverse through the diffusion boundary layer or after they reach the bulk solution (Pena and Miller, 2006). From kinetic studies of n-C_{10} solubilization by micellar solutions of sodium dodecyl sulfate (SDS) it was found that the solubilization rate was dictated not by the diffusion of oil molecules in the water solution but rather by the resistance to incorporate decane molecules from the bulk solution into the micelles (Todorov et al., 2002). Despite the up-to-date research advances on the experimental investigation and numerical modeling of hydrocarbon recovery with surfactant flushing (Mulligan et al., 2001; Sahloul et al., 2002), there is still an ambiguity concerning the interactions of oil dissolution with oil mobilization (Chrysikopoulos and Vogler, 2006) and their individual contribution to the global oil recovery efficiency under conditions favoring both mechanisms. The present study is an attempt to elucidate the interactive effects of oil dissolution and mobilization into a porous medium by (i) monitoring the transient evolution of n-C_{10} saturation along five successive segments of a soil column and dissolved n-C_{10} concentration in water effluent, (ii) formulating a mathematical model of surfactant enhanced hydrocarbon dissolution-mobilization and (ii) determining explicitly the effective n-C_{10} dissolution rate over each soil segment..

METHODS AND MATERIALS

Experiments were performed on a long vertical soil column (Table 1) equipped with electrodes along its length (Aggelopoulos and Tsakiroglou, 2007, 2008). First, the column was evacuated and filled with brine (aqueous solution of NaCl, C_{NaCl}=17.5 g/L). Then, the soil column was flushed downwards at constant influx rates with (i) n-C_{10} (drainage, flow rate Q_o=3ml/min), (ii) brine (imbibition, flow rate Q_w=0.5ml/min) and (iii) brine mixed with SDS (surfactant flushing, C_{NaCl}=17.5 g/L, C_{SDS}=4.9 g/L, flow rate Q_s=0.5ml/min). It was confirmed that the SDS had negligible effect on the electrical conductance of brine. The drainage and imbibition resistivity index curves were constructed by recording the transient changes of electrical resistivity across five successive segments of the column with the aid of electrodes, and measuring the transient variation of water saturation from the total injected volume and effluent weight (Aggelopoulos et al., 2005; Aggelopoulos and Tsakiroglou, 2007, 2008). The resistivity index curves were furthermore employed to determine the transient variation of brine saturation (and consequently of residual oil saturation) across five successive segments of the soil column during the various steps of the experiment. The imbibition resistivity index was used to produce the water saturation as a function of time for the SDS flushing step. The transformation of resistivity index to water saturation was done by using the non-Archie equation (Aggelopoulos et al, 2005)

$$I_R = aS_w^{-m} + (1-a)S_w^{-n} \quad (1)$$

with the fitting parameters shown in Table 2. In order to eliminate the noise that is embedded into the electrical measurements and hence into the calculated water saturation profiles, the transient response of $<S_w>_{ij}$ in SDS flushing test was denoised with multi-level wavelets (Daubechies, 1992).

Moreover, effluent samples were collected at various times from the column outlet and the n-C_{10} concentration in the aqueous phase was measured with Gas Chromatogrphy-Flame Ionization Detector (GC-FID) coupled with solid phase micro-extraction (SPME). Initially, the dissolved n-C_{10} was adsorbed on a fiber that was sunk in the aqueous solution and agitated for 0.5 hr under constant rotation speed. Afterwards, the fiber was transferred to the GC, where the n-C_{10} was desorbed under

high temperature and its quantity was measured from the peak area with comparison to the peak area of a standard n-C_{10} solution.

RESULTS AND DISCUSSION

The non-uniform water saturation in the lower segments of the soil column, at the end of drainage, can be attributed to the capillary end effect (Fig.2a). Although the axial water saturation profile has the tendency to be homogenized during the imbibition step (Fig.2b) some differences in saturation still remain mainly because the transient displacement pattern is governed by capillary forces and frequent bypass of oil-occupied regions occurs (Tsakiroglou et al., 2003a, 2003b). The surfactant flushing experiment was interrupted after the injection of ~63 PV (pore volumes), when no important change of electrical conductance (and hence of residual oil) was detected any more (Fig.3a). At the beginning, oil trapped on the top of the soil was mobilized, and transferred gradually from the upper to the lower layers where it might be trapped again. This is reflected in the initial reduction and subsequent increase of water saturation in each segment of the soil column (Fig.3a). Afterwards, the water saturation starts increasing slowly (Fig.3a) since the dissolution of n-C_{10} in aqueous phase is a slow mass-transfer process governed by the rate of n-C_{10} diffusion in a boundary layer surrounding the oil/water interface and rate of n-C_{10} molecules incorporation into the micelles (Todorov et al., 2002). As it was noticed earlier, because of the anionic nature of SDS, first the n-C_{10} molecules dissolve in aqueous phase and diffuse in the bulk and then they are captured by micelles. The increase in apparent n-C_{10} solubility in the presence of micelles is due almost entirely to n-C_{10} partitioning into the micellar core, so that the amount of n-C_{10} dissolved in the aqueous phase is essentially unaffected by the presence of surfactants so long as there is any excess of hydrocarbon present. By introducing the GC-FID measurements of n-C_{10} concentration (Fig.3b) into simple mass balances, it was found that only ~0.6% of the initial residual n-C_{10} saturation was dissolved in the aqueous phase. It is reasonable to assume that only a fraction of the total n-C_{10} (that has been dissolved in the aqueous and micelle phases) was extracted with SPME, given that the final variation of water saturation was ~9.6 %. Therefore, most of n-C_{10} withdrawn from the oil phase was transferred either in the micelles or in the oil phase displaced from the porous medium.

The n-C10 dissolution/mobilization in SDS micellar solution is modeled by formulating 1-D mass balances for n-C_{10} in the two-fluid system (oil and aqueous phase) and single-fluid system (aqueous phase) Locally, the water flow rate is not constant because of the flow of mobilized oil phase. Instead of using the classical formulation of Darcy's law and relative permeabilities, the local oil flux ($q_o/\varphi A$) was regarded as a dispersive term by using the approximate relationship

$$\frac{q_o}{\varphi A} = -D_{mob}\frac{\partial S_o}{\partial x} \tag{2}$$

where D_{mob} is a mobilization coefficient depending on the local flow field, and spatial fluid distribution (oil ganglia sizes, shapes, etc) (Payatakes and Dias, 1984), φ is the porosity, A is the cross-sectional area, and S_o is the oil saturation. On the other hand, the global oil dissolution rate (including oil solubilization by micelles) was given by the relation (Grinmberg et al., 1995)

$$J_{dis} = K_{dis}\alpha_i(C_s - C) \tag{3}$$

where K_{dis} is the observed mass-transfer coefficient, α_i is the n-C_{10}/water total specific interfacial area, C_s is the n-C10 apparent solubility (maximum concentration of n-C_{10}

in aqueous and micelle phases), and C is the actual n-C_{10} concentration in aqueous and micelle phases. After some manipulation the following system of coupled non-linear PDEs was obtained

$$\frac{\partial S_o}{\partial t} = \frac{\partial}{\partial x}\left(D_{mob} \frac{\partial S_o}{\partial x} \right) - \frac{K_{dis}\alpha_i}{\rho_o}(C_s - C) \tag{4}$$

$$(1-S_o)\frac{\partial C}{\partial t} = \frac{\partial}{\partial x}\left[D_L (1-S_o)\frac{\partial C}{\partial x} \right] - \frac{Q_s}{\varphi A}\frac{\partial C}{\partial x} - D_{mob}\frac{\partial S_o}{\partial x}\frac{\partial C}{\partial x} + 2C\frac{\partial}{\partial x}\left(D_{mob}\frac{\partial S_o}{\partial x} \right) + K_{dis}\alpha_i\left(1 - \frac{C}{\rho_o} \right)(C_s - C) \tag{5}$$

where D_L is the longitudinal dispersion coefficient (Aggelopoulos and Tsakiroglou, 2007) and the interfacial area is given by $\alpha_i = \alpha_0 S_o^{\beta}$.

The aforementioned system of equations coupled with the adequate initial and boundary conditions could be solved and fitted to experimental data to estimate the various parameters involved. Because of the uncertainties embedded into such multi-parameter estimation procedures, the following simplifying approach was adopted. The volume averaging of the n-C_{10} continuity equation,Eq.(4),over each soil segment yields

$$A\varphi L_{ij}\rho_o \frac{\partial \langle S_o \rangle_{ij}}{\partial t} = -\left[\langle F_{ij} \rangle + \rho_o A\varphi\left(u_{o,j}S_{o,j} - u_{o,i}S_{o,i} \right) \right] = -\langle EDR \rangle_{ij} \tag{6}$$

where L_{ij} is the length of segment ij, the term $\rho_o A\varphi\left(u_{o,j}S_{o,j} - u_{o,i}S_{o,i} \right)$ expresses the net rate of n-C_{10} mass outflow (and is equal to the change of the n-C_{10} mobilization rate), the term $\langle F_{ij} \rangle$ is the actual dissolution rate averaged over the segment ij, whereas $\langle EDR \rangle_{ij}$ is the effective dissolution rate averaged over each segment ij. Based on Eq.(6), the time derivative of the water saturation averaged over each segment (Fig.3a) was calculated explicitly and the corresponding <EDR> was determined (Fig.4). At early times (t<100min) the process is dominated by relatively slow and non-uniform mobilization, and is reflected in high $<EDR>_{ij}$ values particularly with reference to the upper segments (Fig.4a). At late times (t>200min), n-C_{10} dissolution becomes dominant, n-C10 ganglia may be mobilized at low rates only over the lower segments, whereas in the upper layers the n-C10 ganglia are stranded (Fig.4b).

CONCLUSIONS

An experimental technique was developed to monitor the transient evolution of the axial water saturation profile in a soil column during the dissolution/mobilization of hydrocarbons by surfactant aqueous solutions. An aqueous solution of NaCl and anionic surfactant SDS at concentration higher than the CMC, as well as n-C_{10} were used. A multi-point resistivity meter was used to record continuously the resistivity index of five successive segments of the soil column and a non-Archie equation was employed to transform the resistivity values to water saturation. Because of the partition of dissolved n-C_{10} in aqueous and micelle phases we were unable to dictate the total concentration of dissolved n-C_{10} by coupling SPME with GC-FID. The effective n-C_{10} dissolution rate $<EDR>_{ij}$, calculated explicitly over each soil segment by employing the experimental data is a fingerprint of the competitive mechanisms and indicates that oil mobilization is dominant over the upper segments at early times while oil dissolution in aqueous and micelle phases is evident throughout the soil column at late times.

REFERENCES

1. Aggelopoulos, C., P. Klepetsanis, M. Theodoropoulou, K. Pomoni, and C.D. Tsakiroglou "Large-scale effects on the resistivity index of porous media", *J. Contam. Hydrology*, **77,** 299-323 (2005).
2. Aggelopoulos, C.A., and C.D. Tsakiroglou, "The longitudinal dispersion coefficient of soils as related to the variability of local permeability", *Water, Air and Soil Pollution*, **185,** 223-237 (2007).
3. Aggelopoulos, C.A., and C.D. Tsakiroglou, "The effect of micro-heterogeneity and capillary number on capillary pressure and relative permeability curves of soils", *Geoderma*, **148**, 25-34 (2008).
4. Chrysikopoulos, C.V., and E.T. Vogler, "Acoustically enhanced ganglia dissolution and mobilization in a monolayer of glass beads", *Transp. Porous Media* (2006) **64**, 103-121.
5. Daubechies, I, "The lectures on Wavelets", SIAM, Philadelphia, 1992.
6. Grimberg, S.J., J. Nagel, and M.D. Aitken, "Kinetics of phenanthrene dissolution into water in the presence of non-ionic surfactants", *Environ, Sci. Technol.* (1995) **29**, 1480-1487.
7. Khachikian, C., and T.C. Harmon, "Nonaqueous phase liquid dissolution in porous media: current state of knowledge and research needs", *Transp. Porous Media* (2000) **38**, 3-28.
8. Mulligan, C.N., R.N. Yong, and B.F. Gibbs, "Surfactant-enhanced remediation of contaminated soil: a review", *Eng. Geol.* (2001) **60**, 371-380.
9. Payatakes, A.C., and M.M. Dias, "Immiscible microdisplacement and ganglion dynamics in porous media", *Rev. Chem. Eng.* (1984) **2**, 85-174.
10. Pena, A.A., and C.A. Miller, "Solubilization rates of oils in surfactant solutions and their relationship to mass transport in emulsions", *Adv. Coll. Interface Sci.* (2006) **123-126**, 241-257.
11. Prak, D.J.L, L.M. Abriola, W.J. Weber, K.A. Bocskay, and K.D. Pennell, "Solubilization rates of n-alkanes in micellar solutions of non-ionic surfactants" *Env. Sci. Technol.* (2000) **34**, 476-482.
12. Sahloul, N.A., M.A. Ioannidis, and I. Chatzis, "Dissolution of residula nonaqueous phase liquids in porous media: poe-scale mechanisms and mass transfer rates", *Adv. Water Resour.* (2002) **25**, 33-49
13. Todorov, P.D., P.A. Kralchevsky, N.D. Denkov, G. Broze, and A. Mehreteab, "Kinetics of solubilization of n-decane and benzene by micellar solutions of sodium dodecyl sulphate", *J. Colloid Interface Sci.* (2002) **245**, 371-382.
14. Tsakiroglou, C.D., M. Theodoropoulou, and V. Karoutsos, "Non-equilibrium capillary pressure and relative permeability curves of porous media", *AIChE J.*, **49,** 2472-2486 (2003a).
15. Tsakiroglou, C.D., M. Theodoropoulou, V. Karoutsos, D. Papanicolaou, V. Sygouni "Experimental study of the immiscible displecement of shear-thinning fluids in pore networks", *J. Colloid Interface Science*, **267,** 217-232 (2003b).
16. Zhou, D., L.A. Dillard, and M. Blunt, "A physically based model of dissolution of nonaqueous phase liquids in the saturated zone", *Transp. Porous Media* (2000) **39**, 227-255.
17. Zhou, W., and L. Zhu, "Solubilization of pyrene by anionic-nonionic mixed surfactants", *J. Hazardous Mat. B* (2004) **109**, 213-220.

Table 1. Properties of soil column

Soil	**S1**
Porosity, φ	0.40
Permeability, k	25.2 D
Formation factor, F	3.97
Soil column length, L	29 cm
Diameter, D	4.75 cm
Mean grain size, $<d_g>$	$2x10^{-2}$ cm

Table 2. Fitting parameter values of resistivity index model

Electrode pair	a		m		n	
	Drainage	Imbibition	Drainage	Imbibition	Drainage	Imbibition
12	0.708	0.918	7.48	6.73	2.02	0.844
13	0.964	0.961	8.54	3.43	0.084	0.128
14	0.943	0.952	12.64	3.68	0.287	0.203
15	0.933	0.955	15.72	3.11	0.299	0.137
16	0.919	0.965	17.84	2.80	0.391	0.0

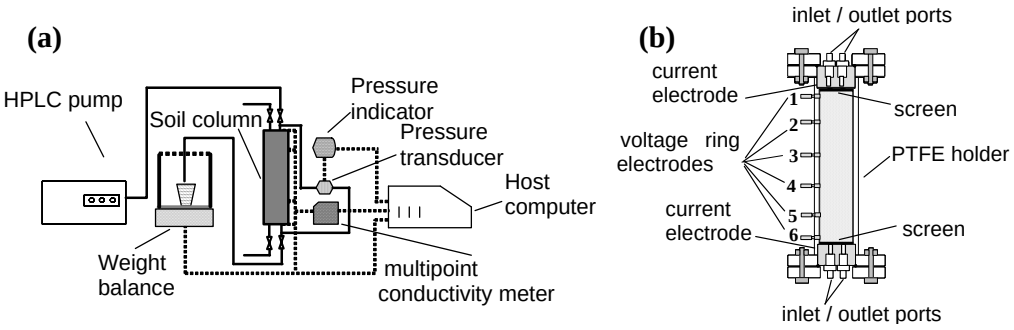

Figure 1. (a) Experimental setup. (b) Schematic diagram of soil column with electrodes

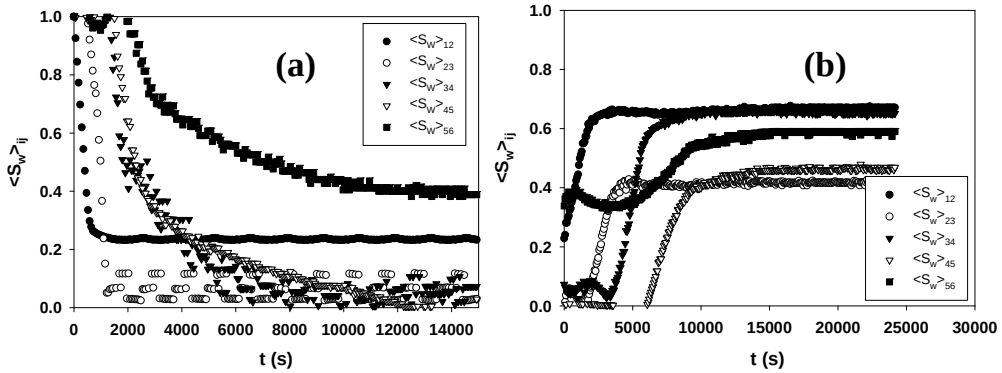

Figure 2. Transient response of water saturation profile during (a) drainage, (b) imbibition steps

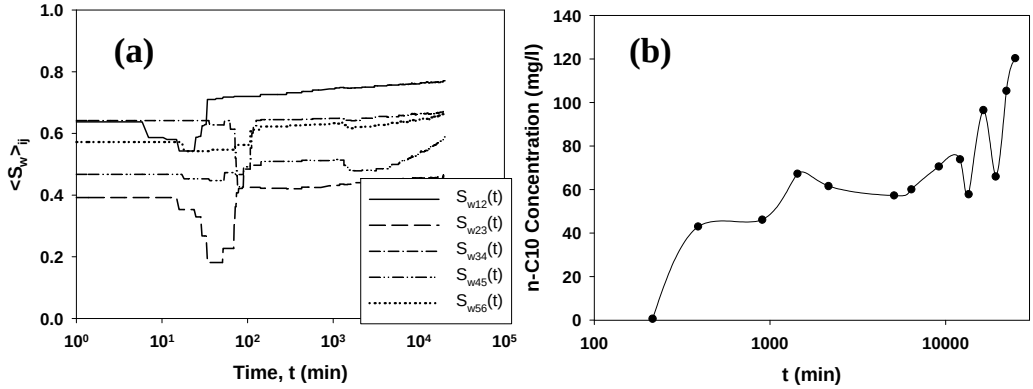

Figure 3. (a) Transient variation of water saturation averaged over five successive segments of the soil column. (b) Transient variation of dissolved n-C_{10} concentration measured with SPME and GC-FID.

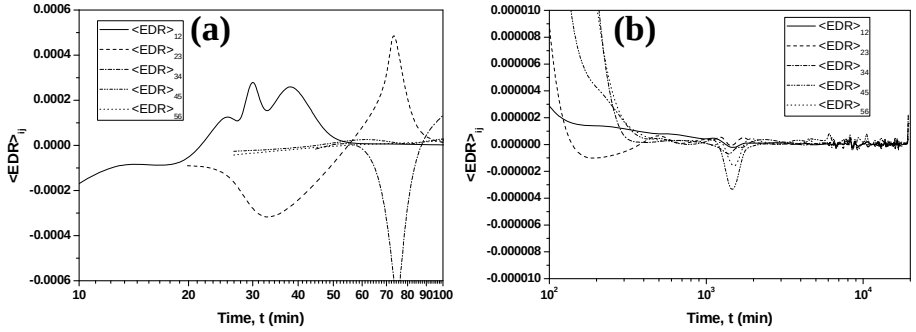

Figure 4. Transient response of the $<EDR>_{ij}$ in each segment at (a) early times, (b) late times